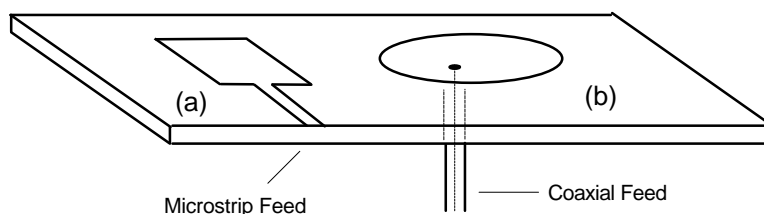


## CHAPTER 5

### THE MICROSTRIP ANTENNA

#### 5.1 Introduction

Applications that require low-profile, light weight, easily manufactured, inexpensive, conformable antennas often use some form of a microstrip radiator. The microstrip antenna (MSA) is a resonant structure that consists of a dielectric substrate sandwiched between a metallic conducting patch and a ground plane. The MSA is commonly excited using a microstrip edge feed or a coaxial probe. The canonical forms of the MSA are the rectangular and circular patch MSAs. The rectangular patch antenna in Figure 5.1 is fed using a microstrip edge feed and the circular patch antenna is fed using a coaxial probe.



**Figure 5.1.** (a) A rectangular patch microstrip antenna fed with a microstrip edge feed. (b) A circular patch microstrip antenna fed with a coaxial probe feed.

The patch shapes in Figure 5.1 are symmetric and their radiation is easy to model. However, application specific patch shapes are often used to optimize certain aspects of MSA performance.

The earliest work on the MSA was performed in the 1950s by Gutton and Baissinot in France and Deschamps in the United States. [1] Demand for low-profile antennas increased in the 1970s, and interest in the MSA was renewed. Notably, Munson obtained the original patent on the MSA, and Howell published the first experimental data involving circular and rectangular patch MSA characteristics. [1] Today the MSA is widely used in practice due to its low profile, light weight, cheap manufacturing costs, and potential conformability. [2]

A number of methods are used to model the performance of the MSA. The simplest model of the MSA is the transmission line model, developed in the 1970s by Munson. [1] The radiating edges of the patch, located at and opposite the feed edge, are modeled as a pair of transmission lines excited  $180^\circ$  out of phase. [1] This method neglects field variations along the radiating edge, and feed effects. Another disadvantage is that an empirically determined correction factor is required to account for fringing fields at the edges of the patch. [1] Despite these assumptions, the transmission line model provides a useful zeroth order approximation to the behavior of the rectangular patch MSA. However, it is not applicable to the circular patch MSA or patches of arbitrary shape. [1]

A more rigorous solution to MSA behavior is the magnetic cavity model. The MSA is modeled as a resonant  $TM_{mn}$  cavity with perfect electrically conducting (PEC) top and bottom surfaces and a perfectly magnetically conducting (PMC) ribbon around the edge. [4] The fields in the antenna are derived by solving for  $TM_{mn}$  modes in the cavity. The radiation is accounted for using a loss tangent in the material, or a reflection coefficient at the PMC ribbon. Within the cavity, the  $TM_{00}$  mode represents static capacitance and loss in the conductors. The  $TM_{10}$  and higher modes are radiative. [1] The magnetic cavity model works well for cavities of simple shape, such as the rectangular and circular patch MSA. However, derivation of the  $TM_{mn}$  modes in an arbitrarily shaped cavity is often tedious. For patch antennas of arbitrary shape, numerical methods are used to solve the integral equations. The Finite Difference Time Domain (FDTD) method and the Method of Moments (MoM) are both applied in practice.

The greatest disadvantage of the MSA is narrow impedance bandwidth. Also, losses in the conductors and substrate cause reduced radiation efficiency. Finally, the classic resonant patch length is on the order of  $\lambda/2$ . This length is restrictive when applications require a compact antenna design.

This discussion involves the analysis and design of the MSA. The classic MSA patch shapes are modeled, and variations on the classic designs are presented that improve certain aspects of performance. Section 5.2 treats the magnetic cavity model, and applies it to the rectangular and circular patch MSAs. Design formulas are derived for both patch shapes. Section 5.3 presents techniques used to widen the impedance bandwidth of the MSA. Also, variations of the rectangular and circular patch shapes are discussed that allow size reduction of the MSA. Concluding remarks are made in Section 5.4.

## **5.2 The Rectangular and Circular Patch Microstrip Antennas**

### **5.2.1 The Magnetic Cavity Model**

One method commonly used to model microstrip antennas is the Magnetic Cavity Model. The cavity model of the MSA assumes that the patch and the ground plane are electric walls, and the periphery of the patch is a magnetic wall. [3] The fields in the resulting cavity are assumed to be the fields of the antenna and Huygen's Principle is applied at the magnetic wall to determine radiation. [3] To determine the fields within the cavity, a solution of an inhomogeneous wave equation is required. Therefore, the Magnetic Cavity Model is most easily applied when the method of separation of variables is applicable. [3] The rectangular and circular patch MSAs are symmetric in two planes. Therefore, the cavity model is convenient in both cases. For arbitrarily shaped patches, application of the Method of Moments to the integral equation is necessary to avoid tedious calculations. [3]

The magnetic cavity model works best for a thin substrate. In this case the TM modes are superior in the cavity. The cavity model makes the following assumptions: [3]

1. The electric field is  $z$ -directed, and the magnetic field has only a transverse component in the cavity.
2. Since the substrate is assumed thin, the fields in the cavity do not vary with  $z$ .
3. The tangential component of the magnetic field is negligible at the edge of the patch.
4. The existence of a fringing field can be accounted for by slightly extending the edges of the patch.

An arbitrarily shaped microstrip patch is illustrated in Figure 5.2. The substrate thickness,  $t$ , is thin. The circumference of the patch is  $C$  and the area bounded by the circumference is  $S$ . The unit vector,  $\mathbf{n}$ , is normal to the patch edge. The substrate has a dielectric constant  $\epsilon_r$ .

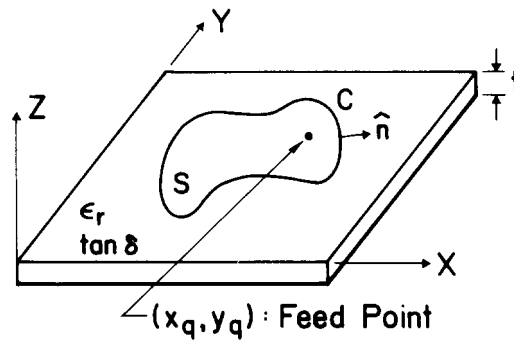


**Figure 5.2.** An arbitrarily shaped microstrip patch antenna

If an  $e^{j\omega t}$  time variation is assumed, the fields from a  $z$ -directed current source at the point  $(x_q, y_q)$  satisfy the following relations: [3]

$$(\nabla_T^2 + k^2)E_z = -j\omega\mu_o J_z(x_q, y_q) \quad (5.1)$$

$$\mathbf{H} = \frac{j}{\omega\mu_o} \nabla_T \times (\mathbf{a}_z E_z) \quad (5.2)$$

where  $\nabla_T$  is the transverse of the del operator with respect to the  $z$ -axis, and

$$k = k_o \sqrt{\epsilon_r} \quad (5.3)$$

where  $k_o$  is the wave number.

Both (5.1) and (5.2) are derived using Maxwell's Equations. The electric wall condition is automatically satisfied at the patch and ground plane because the electric field is defined as perpendicular to both. The magnetic wall condition is satisfied at the edges of the patch if

$$\frac{\partial E_z}{\partial n} = 0 \quad (5.4)$$

The expression in (5.2) is an inhomogeneous wave equation that can be solved by finding eigenfunctions,  $\phi^{(l)}$ , that satisfy the following homogeneous wave equation [3]

$$(\nabla_T^2 + (k^{(l)})^2)\phi^{(l)} = 0 \quad (5.5)$$

for the boundary condition in (5.4). In (5.5),  $k^{(l)}$  is the eigenvalue that corresponds to the eigenvector  $\phi^{(l)}$ . [3] Therefore, if  $N$  modes exist in the cavity and  $N$  eigenvectors are derived, the solution to (5.1) is given by [3]

$$E_z(x, y) = \sum_{l=1}^N A^{(l)} \phi^{(l)}(x, y) \quad (5.6)$$

For an antenna with one input terminal, the values of the coefficients are expressed as [3]

$$A^{(l)} = \frac{\sqrt{2S_e}}{t} \frac{M^{(l)*}}{j\omega C + \frac{1}{j\omega L^{(l)}} + g^{(l)}} I_q \quad (5.7)$$

where

$$M^{(l)} = \sqrt{S_e} \phi^{(l)}(x, y)$$

$$C = \epsilon_r \epsilon_o \frac{S_e}{t}$$

$$L^{(l)} = \frac{1}{(\omega^{(l)})^2 C}$$

and

$$\omega^{(l)} = \frac{k^{(l)}}{\sqrt{\epsilon_r \epsilon_o \mu_o}}$$

In (5.7)  $S_e$  is the effective area of the cavity including the extension due to the fringing fields, and  $g^{(l)}$  is a factor that accounts for conductor, dielectric and radiation loss given by [3]

$$g^{(l)} = g_c^{(l)} + g_d^{(l)} + g_r^{(l)} \quad (5.8)$$

where

$$g_c^{(l)} = \frac{2R_s}{t\mu_o} \left( \frac{\omega^{(l)}}{\omega} \right)^2 C$$

$$g_d^{(l)} = \omega C \tan \delta$$

$$g_r^{(l)} = \frac{2S_e}{t^2} P_{r0}^{(l)}$$

Here,  $R_s$  is the real part of the surface impedance of the patch and ground plane,  $\omega$  is the free space wavelength, and  $P_{r0}^{(l)}$  is given by [3]

$$P_{r0}^{(l)} = \frac{1}{2} \text{Re} \left\{ \iint (\mathbf{E}_0^{(l)*} \times \mathbf{H}_0^{(l)}) \cdot \mathbf{a}_R \sin \theta d\theta d\phi \right\} \quad (5.9)$$

where

$$\mathbf{E}_0^{(l)} = \eta_o \mathbf{H}_0^{(l)} \times \mathbf{a}_R \quad \left( 0 \leq \theta \leq \frac{\pi}{2} \right) \quad (5.10)$$

$$\mathbf{H}_0^{(l)} = \frac{-j\omega\epsilon_o}{4\pi} t \left[ 2 \cos \left( \frac{k_o t}{2} \cos \theta \right) \right] \oint_c (\mathbf{a}_n \times \mathbf{a}_z) \varphi^{(l)}(r) e^{jk\mathbf{r} \cdot \mathbf{R}} dl \quad (5.11)$$

In (5.9)  $\mathbf{a}_R$  is the spherical coordinate unit vector in the  $r$  direction. In (5.10) and (5.11),  $\mathbf{r}$  is a vector from the coordinate origin to a reference point on the periphery of the patch

antenna,  $\varphi^{(l)}(r)$  is the value of the eigenfunction at the end of  $\mathbf{r}$ ,  $\eta_0$  is the impedance of free space, and  $k_0$  is the free space wave number.

For a MSA with a single feed point, the input impedance is given by [3]

$$Z_{in} = \sum_{l=1}^N \frac{|M^{(l)}|^2}{j\omega C + \frac{1}{j\omega L^{(l)}} + g^{(l)}} \quad (5.12)$$

Substituting (5.7) into (5.6) determines the fields of the patch antenna. The expressions in (5.10) and (5.11) give the contributions of each mode in the cavity to the radiating fields. The total radiated field is a sum of the contributions from each resonant mode in the cavity. Expressions for the sum are [3]

$$E_{\theta} = \sum_{l=1}^n A^{(l)} E_0^{(l)} \cdot \mathbf{a}_{\theta} \quad (5.13)$$

$$E_{\phi} = \sum_{l=1}^n A^{(l)} E_0^{(l)} \cdot \mathbf{a}_{\phi} \quad (5.14)$$

where  $\mathbf{a}_{\theta}$  and  $\mathbf{a}_{\phi}$  are the spherical unit vectors.

The directivity at  $\theta = 0^\circ$  is given by [3]

$$U = \frac{|E_{\theta}(\theta = 0^\circ)|^2 + |E_{\phi}(\theta = 0^\circ)|^2}{60P_r} \quad (5.15)$$

and the radiation efficiency of the MSA is [3]

$$\eta = \frac{P_r}{P_c + P_d + P_r} \quad (5.16)$$

where  $P_r$  is the radiated power and  $P_c$  and  $P_d$  are the dissipated power due to conductor and dielectric losses. These quantities are found using [3]

$$P_c = \frac{R_s}{(120\pi)^2} \sum_{l=1}^N |A^{(l)}|^2 \left( \frac{k^{(l)}}{k} \right)^2 = 2\omega \left( \frac{\delta_s}{t} \right) \overline{W}_m \quad (5.17)$$

$$P_d = \frac{t\omega}{2} \epsilon_r \epsilon_o \tan \delta \sum_{l=1}^N |A^{(l)}|^2 = 2\omega (\tan \delta) \overline{W}_e \quad (5.18)$$

$$P_r = \sum_{l=1}^N |A^{(l)}|^2 P_{r0}^{(l)} \quad (5.19)$$

From (5.17) and (5.18), the Q for the conductor and dielectric losses are [3]

$$Q_c = \frac{t}{\delta_s} \quad (5.20)$$

$$Q_d = \frac{1}{\tan \delta} \quad (5.21)$$

The expressions in (5.20) and (5.21) are independent of patch shape. The Q for the radiation loss is [3]

$$Q_r = \omega \frac{0.5 \epsilon \int_v |E_z|^2 dv}{P_{r0}^{(l)}} \quad (5.22)$$

These three factors are combined to derive the radiation Q of the antenna [3]

$$\frac{1}{Q_o} = \frac{1}{Q_r} + \frac{1}{Q_c} + \frac{1}{Q_d} \quad (5.23)$$

This section has presented the magnetic cavity model as a method of analysis applicable to planar microstrip antennas. In the next section, the magnetic cavity model is applied to the rectangular and circular microstrip patch antennas.

## 5.2.2. Application of the Magnetic Cavity Model to the Microstrip Antenna

The rectangular and circular microstrip patch antennas are illustrated in Figure 5.3.

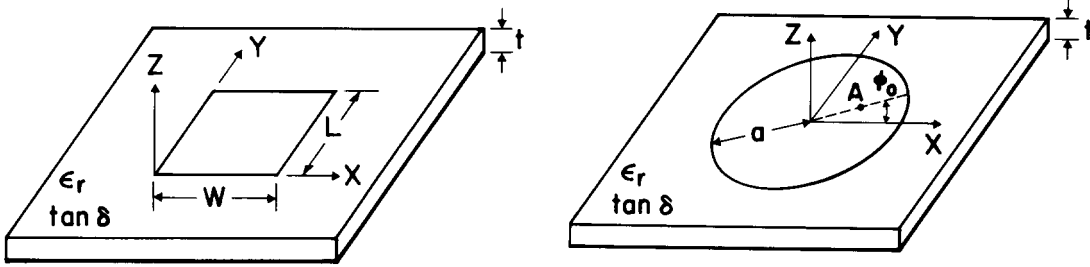


**Figure 5.3.** The dimensions of the (a) rectangular patch antenna and (b) circular patch antenna.

A simple way to model the rectangular patch antenna is to assume the radiating edges, located at and opposite the feed edge, are slots of width  $t$  radiating into a half-space. [3] This is called the transmission line model. However, the transmission line model is not applicable to the circular patch. In addition, it ignores field variations along the radiating edges and feed effects. [3] Therefore, the following discussion applies the magnetic cavity models to the rectangular and circular patch antennas in Figure 5.3.

### 5.2.2.1 The Rectangular Patch Microstrip Antenna

The solution of (5.5) for a rectangular conducting patch of length  $L$  and width  $W$  is [3]

$$\Phi_{mn}(x, y) = \frac{\delta_m \delta_n}{\sqrt{W_e L_e}} \cos\left(\frac{m\pi x}{W_e}\right) \cos\left(\frac{n\pi y}{L_e}\right) \quad (5.24)$$

$$\delta_l = \begin{cases} 1, & l = 0 \\ \sqrt{2}, & l \neq 0 \end{cases}$$

where  $m$  and  $n$  correspond to the mode indices in the  $x$  and  $y$  directions,  $W_e$  is the effective width including the extension used to simulate the fringing fields, and  $L_e$  is the effective length. For the  $TM_{10}$  mode, the effective dimensions are found using [3]

$$W_e = W[1 + \Delta(W)] \frac{\sqrt{\epsilon_e(W)\epsilon_e(L)}}{\epsilon_r} \quad (5.25)$$

$$L_e = L \quad (5.26)$$

and for the  $TM_{01}$  mode using [3]

$$W_e = W \quad (5.27)$$

$$L_e = L[1 + \Delta(L)] \frac{\sqrt{\epsilon_e(W)\epsilon_e(L)}}{\epsilon_r} \quad (5.28)$$

where

$$\epsilon_e(x) = \frac{\epsilon_r + 1}{2} + \frac{\epsilon_r - 1}{2} \left(1 + 10 \frac{t}{x}\right)^{-1/2} \quad (5.29)$$

In these expressions, the  $\Delta$  function is a correction for the effect of the fringing field, and is given by [3]

$$\Delta(x) = \frac{t}{x} \left\{ 0.882 + \frac{0.164(\epsilon_r - 1)}{\epsilon_r} + \frac{\epsilon_r + 1}{\pi\epsilon_r} \left[ 0.758 + \ln\left(\frac{x}{t} + 1.88\right) \right] \right\} \quad (5.30)$$

The eigenvalues are found using [3]

$$k_{mn} = \sqrt{\left(\frac{m\pi}{W_e}\right)^2 + \left(\frac{n\pi}{L_e}\right)^2} \quad (5.31)$$

and are used to derive the resonant frequency with [3]

$$f_{mn} = \frac{k_{mn}}{2\pi\sqrt{\epsilon_r\epsilon_o\mu_o}} \quad (5.32)$$

The electric field in the cavity is found using (5.6), and is given by [3]

$$E_z(x, y) = \sum_m \sum_n \frac{V_{mn}}{t} \cos\left(\frac{m\pi x}{W_e}\right) \cos\left(\frac{n\pi y}{L_e}\right) \quad (5.33)$$

where

$$V_{mn} = \frac{\sqrt{2}(\delta_m\delta_n)^2 I_q}{j\omega C + \frac{1}{j\omega L_{mn}} + g_{mn}} \cos\left(\frac{m\pi x}{W_e}\right) \cos\left(\frac{n\pi y}{L_e}\right) \quad (5.34)$$

The quantities  $C$ ,  $L_{mn}$ , and  $g_{mn}$  are derived using (5.7) through (5.11). The coordinates  $(x_q, y_q)$  give the location of the feed point, and  $I_q$  is the input current.

For a rectangular patch with a single feed point, the input impedance is found using (5.11). The resulting expression is [3]

$$Z_{in} = \sum_m \sum_n \frac{(\delta_m\delta_n)^2}{j\omega C + \frac{1}{j\omega L_{mn}} + g_{mn}} \cos^2\left(\frac{m\pi x}{W_e}\right) \cos^2\left(\frac{n\pi y}{L_e}\right) \quad (5.35)$$

Finally, the radiating fields of the antenna are found by substituting (5.32) into (5.13) and (5.14). The resulting expressions for the radiation patterns of a rectangular MSA are [3]

$$\begin{aligned}
E_{\theta}(\theta, \phi) &= \frac{e^{-jk_o R}}{R} \frac{k_o^2}{2\pi} \left[ \cos\left(\frac{k_o t}{2} \cos\theta\right) \right] \sin\phi \cos\phi \sin\theta \\
&\cdot \sum_m \sum_n V_{mn} \left[ 1 - (-1)^m e^{jk_o W_e \cos\phi \sin\theta} \right] \left[ 1 - (-1)^n e^{jk_o L_e \sin\phi \sin\theta} \right] \\
&\cdot \left\{ \left[ \frac{1}{k_o^2 \cos^2\phi \sin^2\theta - \left(\frac{m\pi}{W_e}\right)^2} \right] + \left[ \frac{1}{k_o^2 \sin^2\phi \sin^2\theta - \left(\frac{n\pi}{L_e}\right)^2} \right] \right\}
\end{aligned} \tag{5.36}$$

and

$$\begin{aligned}
E_{\phi}(\theta, \phi) &= \frac{e^{-jk_o R}}{R} \frac{k_o^2}{2\pi} \left[ \cos\left(\frac{k_o t}{2} \cos\theta\right) \right] \cos\theta \sin\theta \\
&\cdot \sum_m \sum_n V_{mn} \left[ 1 - (-1)^m e^{jk_o W_e \cos\phi \sin\theta} \right] \left[ 1 - (-1)^n e^{jk_o L_e \sin\phi \sin\theta} \right] \\
&\cdot \left\{ \left[ \frac{\sin^2\phi}{k_o^2 \sin^2\phi \sin^2\theta - \left(\frac{n\pi}{L_e}\right)^2} \right] - \left[ \frac{\cos^2\phi}{k_o^2 \cos^2\phi \sin^2\theta - \left(\frac{m\pi}{W_e}\right)^2} \right] \right\}
\end{aligned} \tag{5.37}$$

This completes the application of the magnetic cavity model to a rectangular patch shape.

### 5.2.2.2 The Circular Patch Microstrip Antenna

The magnetic cavity model is also readily applied to a circular patch antenna of radius  $a$ , and feed point location  $A$ , as illustrated in Figure 5.3(b). In this case the solution to (5.5) is given by [3]

$$\varphi_{mn}(r, \phi) = \frac{\delta_m k_{mn}}{\chi_{mn} \sqrt{\pi \left(1 - \frac{m^2}{\chi_{mn}^2}\right)} J_m(\chi_{mn})} J_m(k_{mn} r) \cos(m(\phi - \phi_o)) \tag{5.38}$$

where  $k_{mn}$  is the eigenvalue corresponding to mode  $\text{TM}_{mn}$ , and  $\chi_{mn}$  is the  $n$ th root of

$$J_m'(\chi_{mn}) = 0$$

The prime refers to the derivative on the argument. The function  $J_m(x)$  is the Bessel function of order  $m$ . Some values of  $\chi_{mn}$  are found in Table 5.1.

**Table 5.1.** Some lower roots of  $J_m'(\chi_{mn})$  [3]

	n = 0	n = 1	n = 2	n = 3
m = 1	3.832	1.841	3.054	4.201
m = 2	7.016	5.331	6.706	8.015

The values of  $\chi_{mn}$  are used to find the eigenvalues,  $k_{mn}$ , using [3]

$$k_{mn} = \frac{\chi_{mn}}{a_{mn}} \quad (5.39)$$

where  $a_{mn}$  is the effective patch radius, lengthened to account for fringing fields at the edge of the patch. The eigenvalues are used in (5.32) to find resonant frequency.

Once again, the cavity electric field is found by substituting solutions to (5.38) into (5.6) and (5.7). The expression for the electric field in the cavity is [3]

$$E_z(r, \phi) = \sum_m \sum_n \frac{V_{mn}}{t} \frac{J_m(k_{mn}r)}{J_m(\chi_{mn})} \cos(m(\phi - \phi_o)) \quad (5.40)$$

where

$$V_{mn} = \frac{\sqrt{2}\delta_m^2 I_q}{j\omega C + \frac{1}{j\omega L_{mn}} + g_{mn}} \left( \frac{J_m(k_{mn}r)}{J_m(\chi_{mn})} \right) \left( \frac{1}{1 - \left( \frac{m^2}{\chi_{mn}^2} \right)} \right) \quad (5.41)$$

and the variables are identical to those used for the rectangular patch except that the feed point is denoted using the cylindrical coordinates  $(r, \phi)$ .

The input impedance of the circular patch antenna is found using (5.11) and is given by [3]

$$Z_{in} = \sum_m \sum_n \frac{\delta_m^2}{\left[ j\omega C + \frac{1}{j\omega L_{mn}} + g_{mn} \right] \left[ 1 - \left( \frac{m^2}{\chi_{mn}^2} \right) \right]} \left( \frac{J_m(k_{mn}r)}{J_m(\chi_{mn})} \right) \quad (5.42)$$

And finally, from (5.13) and (5.14), the radiated fields are [3]

$$E_\theta(\theta, \phi) = \frac{e^{-jk_o R}}{R} \frac{\pi}{\lambda_o} \left[ \cos\left(\frac{k_o t}{2} \cos\theta\right) \right] \cdot \sum_m \sum_n a_{mn} V_{mn} e^{j(m\pi/2)} \cos(m(\phi - \phi_o)) \cdot \left[ J_{m+1}(k_o a_{mn} \sin\theta) - J_{m-1}(k_o a_{mn} \sin\theta) \right] \quad (5.43)$$

and

$$E_\phi(\theta, \phi) = \frac{e^{-jk_o R}}{R} \frac{\pi}{\lambda_o} \left[ \cos\left(\frac{k_o t}{2} \cos\theta\right) \right] \cos\theta \sum_m \sum_n a_{mn} V_{mn} e^{j(m\pi/2)} \sin(m(\phi - \phi_o)) \cdot \left[ J_{m+1}(k_o a_{mn} \sin\theta) - J_{m-1}(k_o a_{mn} \sin\theta) \right] \quad (5.44)$$

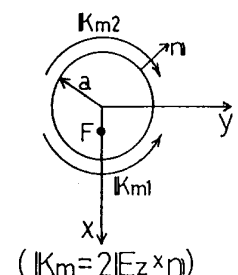
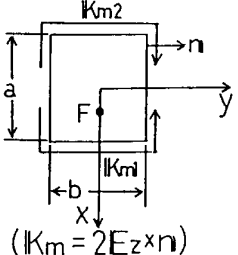
This section has treated the circular patch microstrip antenna using the magnetic cavity model. In the next section, the results of the magnetic cavity model for the rectangular and circular microstrip patch antennas are summarized.

### 5.2.3 Summary of the Magnetic Cavity Model Results

Expressions for the radiation patterns of the rectangular and circular patch MSAs are summarized in Table 5.2. The patterns are for the dominant modes within a thin

substrate. The indices of the dominant mode are noted in the table. Table 5.2 includes illustrations of geometry, expressions of fields within the magnetic cavity, and expressions of the radiated electric and magnetic fields.

**Table 5.2.** Summary of field and radiation pattern results for microstrip patch antennas analyzed using the magnetic cavity model. [4]

Element shape	Expressions of electromagnetic fields	Expressions of radiation pattern
 <p>(<math> K_m  = 2 E_z \times n </math>)</p>	<p>TM<sub>110</sub> mode (Dominant mode)</p> $\begin{cases} E_z = E_0 J_1(k\rho) \cos\phi \\ H_\rho = -\frac{j\omega\epsilon}{k^2} E_0 \frac{J_1(k\rho)}{\rho} \sin\phi \\ H_\phi = -\frac{j\omega\epsilon}{k} E_0 J_1'(k\rho) \cos\phi \end{cases}$	$E_\theta = -jK_d a \cos\phi \sin(m) \left\{ \frac{J_1'(n)}{\cos\theta} \right\}$ $E_\phi = \left( \frac{jK_d}{k_0} \right) \sin\phi \cos(m) \left\{ \frac{J_1(n)}{\cos\theta} \right\}$ $\begin{cases} m = k_0 h \cos\theta \\ n = k_0 a \sin\theta \\ K_d = E_0 \frac{e^{-jk_0 R}}{R} J_1(ka) \end{cases}$
 <p>(<math> K_m  = 2 E_z \times n </math>)</p>	<p>Tm<sub>100</sub> mode (Dominant mode)</p> $\begin{cases} E_z = E_0 \sin\left(\frac{\pi}{a} x\right) \\ H_y = jE_0 \frac{\pi}{\omega\mu_0 a} \cos\left(\frac{\pi}{a} x\right) \end{cases}$	$E_\theta = -jK_r f(\theta, \phi) \cos\phi \left\{ \frac{\epsilon_r - \sin^2\theta}{\epsilon_r - (\sin\theta \cos\phi)^2} \right\}$ $E_\phi = jK_r f(\theta, \phi) \cos\theta \sin\phi \times \left\{ \frac{\epsilon_r}{\epsilon_r - (\sin\theta \cos\phi)^2} \right\}$ $f(\theta, \phi) = \left\{ \frac{\sin(m)}{m} \right\} \cos(n)$ $m = \left(\frac{k_0 b}{2}\right) \sin\theta \sin\phi, \quad n = \left(\frac{k_0 a}{2}\right) \sin\theta \cos\phi$ $K_r = \left(\frac{V_0 k_0 b}{\pi}\right) \frac{e^{-jk_0 R}}{R}, \quad V_0 = E_0 h$

The patterns calculated using the expressions in Table 5.2 are illustrated in Figure 5.4. The patterns are those of a rectangular patch antenna with resonant length of  $0.49\lambda$  and a width of  $0.41\lambda$ . The thickness of the substrate is  $0.025\lambda$ , and the dielectric constant of the substrate is 2.55. The measurements were made against a large ground plane of width  $W_g = 2.04\lambda$  and length  $L_g = 2.73\lambda$ .

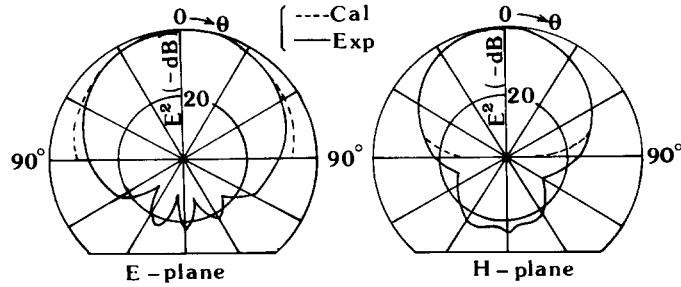


**Figure 5.4.** Modeled and measured radiation patterns of a rectangular microstrip patch antenna using the equations in Table 5.2. [4]

The measured and modeled input impedance of a rectangular microstrip patch over a 20% impedance bandwidth is shown in Figure 5.5. The impedance is calculated using (5.35). The dimensions of the antenna are specified in the plot.

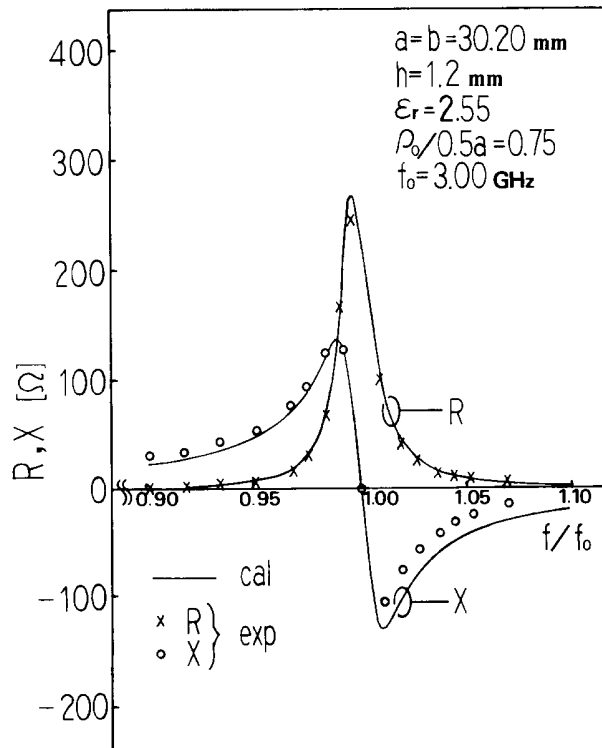


**Figure 5.5.** The measured (points) and calculated (curves) input impedance of a rectangular microstrip patch antenna [4]

The impedance illustrated in Figure 5.5 is characteristic of a high Q antenna because the reactance varies sharply with frequency around resonance. A design curve that relates radiation Q, found in (5.23), and radiation efficiency, found in (5.16), to substrate thickness,  $t$ , is illustrated in Figure 5.6.

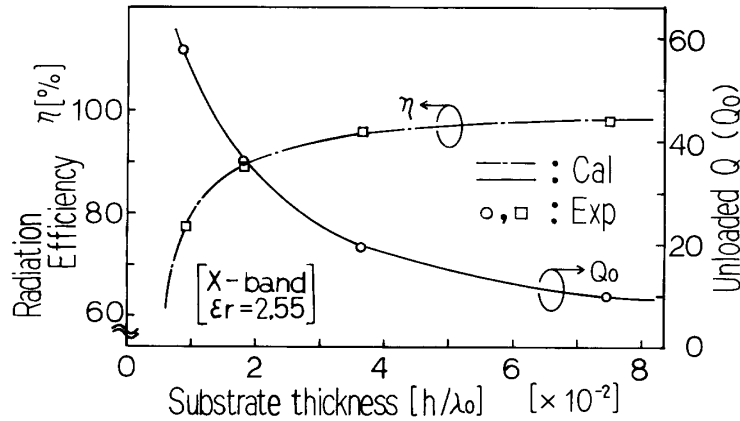


**Figure 5.6.** Radiation efficiency,  $\eta$ , and unloaded radiation Q,  $Q_0$ , as a function of substrate thickness [4]

Figure 5.6 shows that a microstrip patch that uses a thicker substrate is more efficient. In addition, as the substrate thickness increases, the radiation Q of the antenna decreases. Thus, impedance bandwidth increases with increasing substrate thickness. The plot assumes a lossless material with a dielectric constant of 2.55. It is also assumed that the substrate is not thick enough to support surface waves and modes higher than the fundamental mode. As the impedance bandwidth of a MSA increases, the VSWR,  $S$ , at resonance also increases. The relationship between  $BW$  and  $S$  is described by [4]

$$BW = \frac{(S - 1)}{Q_0 \sqrt{S}} \quad (5.45)$$

where  $S$  is the input VSWR at resonance, and  $Q_0$  is the unloaded radiation Q. The expression in (5.45) shows that antennas with lower VSWR and higher Q have narrower

impedance bandwidth. A design can be optimized for bandwidth by selecting substrate thickness using Figure 5.6 and adjusting VSWR.

The resonant frequencies of the rectangular and circular microstrip patch antennas, derived using (5.32), are given in Table 5.3. The table also contains correction factors that account for fringing fields at the edges of the patch. For the rectangular patch, the correction factor is applied to the length of the antenna. For the circular patch, the correction factor is applied to radius.

**Table 5.3.** Resonant lengths and geometrical correction factors for the rectangular and circular microstrip patch antennas. [4]

Circular MSA	$f_r = \frac{\chi_{11} C_0}{2\pi a_{\text{eff}} \sqrt{\epsilon_r}}$ $\begin{cases} \chi_{11} = 1.841 \\ C_0 : \text{light velocity} \\ a_{\text{eff}} = a \left\{ 1 + \frac{2h}{\pi a \epsilon_r} (\ln \frac{\pi a}{2h} + 1.7726) \right\}^{\frac{1}{2}} \end{cases}$
Rectangular MSA	$f_r = \frac{C_0}{2a_{\text{eff}} \sqrt{\epsilon_e}}$ $\begin{cases} \epsilon_r : \text{dielectric constant} \\ a_{\text{eff}} = a \left\{ 1 + 0.824 \frac{h}{a} \frac{(\epsilon_e + 0.3)(a/h + 0.262)}{(\epsilon_e - 0.258)(a/h + 0.813)} \right\} \\ \epsilon_e = \frac{\epsilon_r + 1}{2} + \frac{\epsilon_r - 1}{2} \left( 1 + 10 \frac{h}{a} \right)^{-\frac{1}{2}} \end{cases}$

The expressions in Table 5.3 depend on substrate dielectric constant. Substrates with high dielectric constants allow patch antennas to have smaller resonant dimensions. Thus, in terms of size reduction, a high dielectric constant is desirable. However, material substrates with high dielectric constants tend to support surface waves even when they are thin. These waves reflect from the interface at the edge of the substrate and interfere with

the primary radiator. In array situations, the surface waves cause cross-talk between elements. [4]

The dielectric constant of the substrate also affects the directivity of the MSA. Antennas with higher dielectric constant experience lower directivity. The relation between substrate dielectric constant and directivity is illustrated in Figure 5.7 which shows that the directivity of the MSA is between 5 and 10 dB and is lower for substrates with higher dielectric constant. [4]

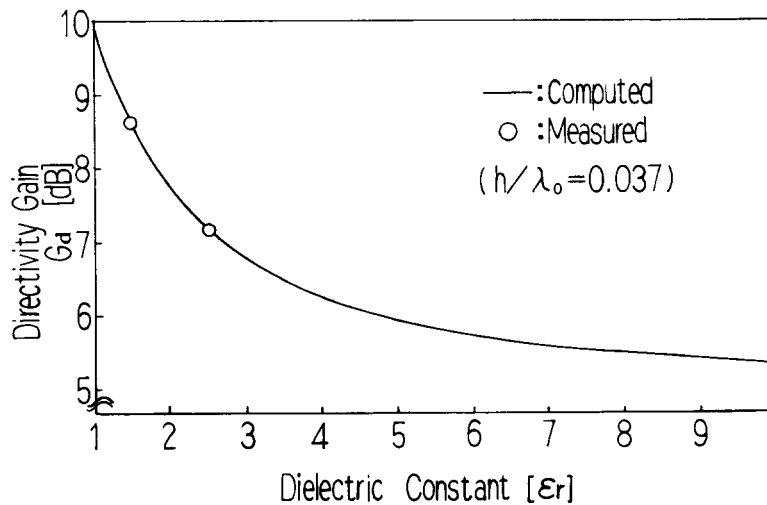


**Figure 5.7.** The directivity of a microstrip antenna as a function of dielectric constant computed using (5-36) and (5-37). [4]

This section has applied the theory of the magnetic cavity model to the rectangular and circular patch antennas. The derived formulas were used to present curves describing fundamental trade-offs in MSA design. However, although the rectangular and circular patch MSAs are symmetrical and easy to fabricate, they are intrinsically high Q. Thus, they have narrow impedance bandwidth. In addition, the performance of the MSA is optimized when a thick substrate with low dielectric constant is used. This has detrimental effects on antenna size reduction. The next section presents methods used to increase the impedance bandwidth and decrease the resonant dimensions of the MSA.

## **5.3. Broad Band Microstrip Antennas**

### **5.3.1 Introduction**

The greatest disadvantage of the microstrip antenna (MSA) is its inherently low impedance bandwidth. The pattern bandwidth of the MSA is much wider than the impedance bandwidth, which can be as low as 1%. [5,6] Since many wide-band applications require a low-profile conformal antenna, much work has gone into designing wide-band MSA elements or producing MSAs with a dual resonance characteristic. However, most microstrip elements that achieve greater bandwidth do so at the cost of increased height or overall volume. [5] This section summarizes some of the general techniques used to increase the bandwidth of the MSA. In addition, the advantages and costs of each technique are presented.

### **5.3.2 Optimizing the Substrate Properties for Increased Bandwidth**

The easiest way to increase the bandwidth of an MSA is to print the antenna on a thicker substrate. [1] However, thick substrates tend to trap surface wave modes, especially if the dielectric constant of the substrate is high. [5] In addition, longer coaxial probe feeds will experience high inductive feed effects. [7] Finally, if the substrate is very thick, radiating modes higher than the fundamental will be excited. [5] All of these effects degrade the primary radiator, cause pattern distortion, and detune the input impedance of the MSA. [5]

Another way to increase the bandwidth of an MSA is to decrease the dielectric constant of the substrate. [5] However, this has detrimental effects on antenna size reduction since the resonant length of an MSA is shorter for higher substrate dielectric

constant. In addition, the directivity of the MSA depends on the dielectric constant of the substrate. This concept was discussed in the previous section.

### 5.3.3 Stacked Microstrip Patch Antennas

Another method commonly used to increase the bandwidth of the MSA is to stack two patches on top of each other separated by a dielectric substrate or spacers. This method was introduced shortly after the introduction of the MSA using stacked circular disks. [8] A similar application was discussed recently for application to MobilSat systems in Australia. [2] The application involved two identical circular patches stacked on top of each other. The lower patch was fed using a coaxial probe feed, and the top patch was electromagnetically coupled to the lower one. The resulting electromagnetically coupled (EMC) MSA is illustrated in Figure 5.8.

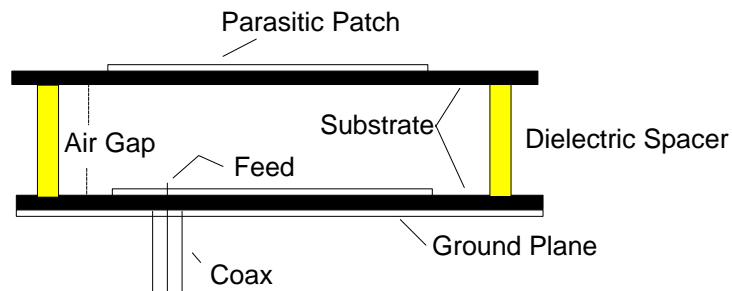


**Figure 5.8.** A stacked circular patch EMC-MSA fed using a coaxial probe.

The specifications of an antenna like that in Figure 5.8 built for the MobilSat application are given in Table 5.4.

The EMC-MSA specified in Table 5.4 was built and the input impedance was measured. [2] The results of the measurement are illustrated in Figure 5.9 which shows that the impedance bandwidth below 10 dB return loss for the EMC-MSA is about 5.6%. [2] The bandwidth for the lower patch alone was measured as 1.13%, so the stacked configuration leads to a significant improvement of impedance bandwidth. Further improvement of the impedance bandwidth is possible by decreasing the diameter of the parasitic patch. Using this technique, bandwidths of up to 13% are possible. [2] The

bandwidth improvement achieved by the EMC-MSA is at the cost of increased antenna height, and overall volume. The circular EMC-MSA is more than 14 times taller than a circular patch of the same diameter.

**Table 5.4.** Specifications of a circular patch EMC-MSA for a MobilSat application

Quantity	Value	Unit
Resonant Frequency	1.62	GHz
Parasitic Patch Diameter	68	mm
Fed Patch Diameter	68	mm
Substrate	Cuclad 250 GX	--
Dielectric Constant	2.55	--
Substrate Thickness	1.524	mm
Air Gap Thickness	20.5	mm

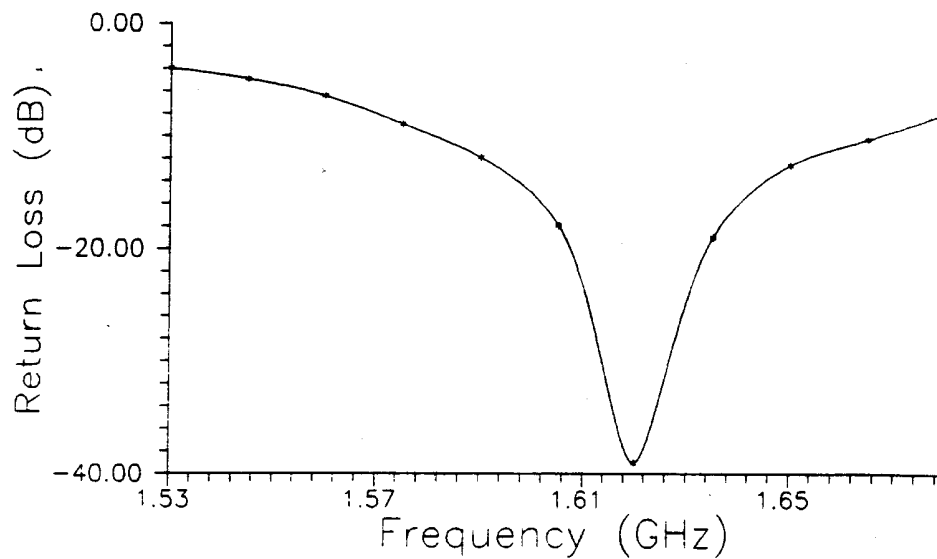


**Figure 5.9.** The measured return loss for the EMC-MSA specified in Table 5.4. [2]

When two patches are stacked on top of each other, the distance between them,  $s$  in Figure 5.10, effects the antenna performance. Closely spaced stacked patches

experience improved impedance bandwidth. For increased separations, the parasitic patch tends to act as a director, and improve the gain, instead of the bandwidth, of the antenna. [9]

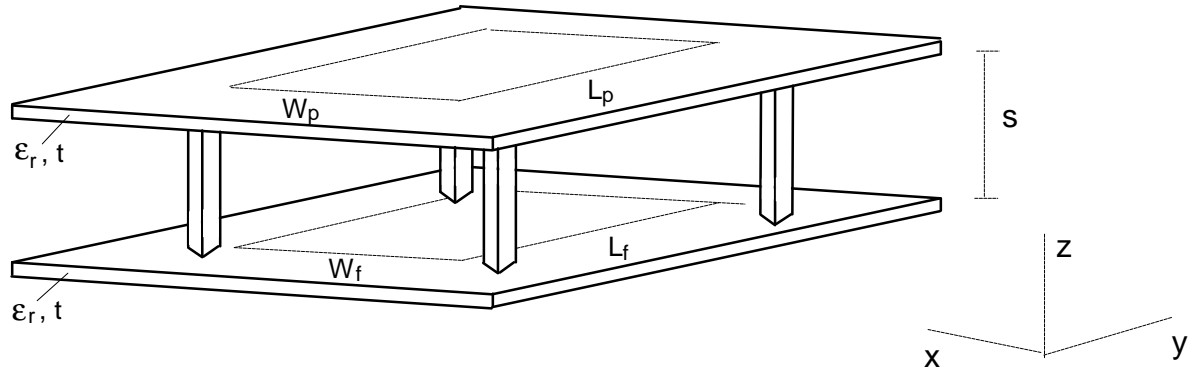


**Figure 5.10.** A stacked microstrip patch antenna using dielectric spacers.

It is possible to categorize the spacing,  $s$ , between stacked patch antennas in Figure 5.10 into three regions. Region 1 extends from  $s = 0$  to  $s = 0.14\lambda$ . This is the improved bandwidth region. The parasitic patch acts as another resonant antenna with a resonant frequency close to that of the fed patch. The result is a wider impedance bandwidth. [9] Region 2 extends from  $s = 0.14\lambda$  to  $s = 0.29\lambda$ . In this region, the radiation patterns of the antenna become irregular. Specifically, the H-Plane pattern becomes unsymmetrical and the E-Plane pattern shows a dip at broadside. [9] Antennas in region 3 ( $s > 0.30\lambda$ ) experience a impedance bandwidth of about 1%, but have broadside gains that approach 10 dB. This is called the high gain region. A stacked rectangular patch EMC-MSA configuration similar to that illustrated in Figure 5.8 was built to demonstrate the effects of the spacing regions. The specifications of the antenna system are given in Table 5.5. The location of the feed on the lower patch in Figure 5.10 is

$$x_{feed} = (0.75)W_f \quad \text{and} \quad y_{feed} = (0.25)L_f$$

The resonant frequencies, 3 dB beamwidths, gains and impedance bandwidths of rectangular stacked EMC-MSAs with different air gap spacings,  $s$ , were measured. The results are given in Table 5.6. [9] Table 5.6 includes values of  $s$  that fall in each of the three regions. The first nine designs are built for high impedance bandwidth ( $0 < s < 0.14\lambda$ ). The last four are built for high gain ( $s > 0.30\lambda$ ). The middle five fall in region 2 ( $0.14\lambda < s < 0.29\lambda$ ).

**Table 5.5.** Specifications of a rectangular stacked EMC-MSA used to determine the effects of different air gap thicknesses.

Quantity	Symbol	Value	Unit
Resonant Frequency	$f_r$	10	GHz
Parasitic Patch Length	$L_p$	10	mm
Parasitic Patch Width	$W_p$	15	mm
Fed Patch Length	$L_f$	10	mm
Fed Patch Width	$W_f$	15	mm
Substrate		Cuflon	--
Dielectric Constant	$\epsilon_r$	2.17	--
Substrate Thickness	$t$	0.254	mm
Air Gap Thickness	$s$	varies	--

**Table 5.6.** Characteristics of rectangular stacked EMC-MSA designs falling into each of the three spacing regions. [9]

Spacing $s$ (cm)	$f_{01}$ (GHz)	Pattern shape	3dB beamwidth (deg.) E x H	Estimated gain (dBi)	Bandwidth %
0.000	9.90	normal	95 x 73	5.7	9.0
0.051	9.95	normal	75 x 65	7.3	13.0
0.102	10.10	normal	75 x 70	7.0	10.5
0.152	10.45	normal	75 x 70	7.0	6.2
0.204	10.46	normal	75 x 70	7.0	4.8
0.254	10.48	normal	70 x 70	7.2	3.4
0.305	10.46	normal	73 x 78	6.6	2.9
0.356	10.46	normal	75 x 85	6.1	2.9
0.406	10.40	normal	85 x 90	5.3	2.6
0.457	10.37	abnormal	-----	---	---
0.508	10.37	abnormal	-----	---	---
0.610	10.34	abnormal	-----	---	---
0.762	10.30	abnormal	-----	---	---
0.864	10.30	abnormal	-----	---	---
0.914	10.28	normal	90 x 37	8.9	1.3
0.965	10.28	normal	90 x 37	8.9	1.3
1.016	10.28	normal	85 x 37	9.2	1.3
1.118	10.30	normal	70 x 37	10.0	1.2
<b>Single patch</b>	<b>10.20</b>	<b>normal</b>	<b>110 x 70</b>	<b>5.3</b>	<b>2.3</b>

Table 5.6 shows that EMC-MSAs with air gap thicknesses falling within region 1 ( $0 < s < 0.14\lambda$ ) experience impedance bandwidths of up to 13% of the center frequency,  $f_{01}$ . This is in agreement with the predictions in [2]. As the spacing increases, the impedance bandwidth of the antenna decreases. In region 2 ( $0.14\lambda < s < 0.29\lambda$ ) the radiation patterns of the antenna become abnormal. In region 3 ( $s > 0.30\lambda$ ), the impedance bandwidth of the antenna is small, but the gain improves to about 10 dB at broadside. [9]

### 5.3.4. Non-contacting Feed Configurations

Another method used to increase the impedance bandwidth of the MSA is the non-contacting feed. The proximity feed shown in Figure 5.11 uses a stacked two layer substrate with the patch printed on the top side of the upper substrate, or superstrate. The feed line is located on the top surface of the lower substrate, and the ground plane is on

the bottom surface of the lower substrate. [10] The location and length of the open-circuit capacitive shunt stub on the feedline is used to tune the input impedance of the antenna.

[10]

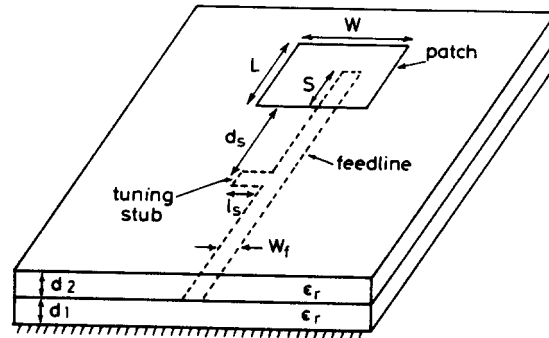


**Figure 5.11.** A proximity fed rectangular patch MSA with a shunt tuning stub. [10]

In Figure 5.11, the patch is of length  $L$  and width  $W$ . The feedline is located under the superstrate and is inset a distance  $S$  with respect to the radiating edge of the patch. The tuning stub is of length  $l_s$  and is located a distance  $d_s$  from the radiating edge of the patch. The substrate has a thickness  $d_1$  and a dielectric constant  $\epsilon_r$ . The superstrate has a thickness  $d_2$ , and an identical dielectric constant. The proximity feed does not directly contact the patch element. Therefore, it is easy to adjust the location of the feed. In addition, the proximity feed allows at least two additional degrees of freedom to tune the antenna, the substrate thickness between the line and the patch,  $d_2$ , and the location of the line with respect to the patch,  $S$ . [10] These dimensions are adjusted to tune the antenna for optimum bandwidth. The location,  $d_s$ , and length,  $l_s$ , of the shunt stub also tune the input impedance of the antenna. It is important to make the tuning stub as short as possible because longer stub lengths, especially those approaching  $\lambda/4$  or  $\lambda/2$ , will cause undesirable radiation. [11]

An antenna like that illustrated in Figure 5.12 was built using the specifications in Table 5.7. [11]

**Table 5.7.** Specifications of a proximity fed rectangular patch MSA

Quantity	Value	Unit
Resonant Frequency	3.5	GHz
$d_1$	1.58	mm
$d_2$	1.58	mm
Material (both layers)	Duroid	--
$\epsilon_r$	2.20	--
$l_s$	6.5	mm
$d_s$	33	mm
$W_f$	5	mm
L	25	mm
W	40	mm
S	12.5	mm

The antenna specified in Table 5.7 was built and the impedance was measured. The measured results on the Smith chart are shown in Figure 5.12. [11] The diameter of the impedance locus in Figure 5.12 is determined by the feedline inset,  $S$ , and the width of the patch,  $W$ . The diameter is greatest when  $S = L/2$ . If the phase reference of the impedance measurement is moved down the transmission line a distance on the order of  $\lambda/2$ , the impedance locus indicates a double resonance characteristic. [11] However, the locus is not centered on the chart. Thus, the short capacitive tuning stub is added at this point to center the locus. The result is the solid impedance characteristic shown in Figure 5.12 that signifies wide-band operation. The bandwidth below  $VSWR = 2$  is between 3.375 and 3.855 GHz, corresponding to an impedance bandwidth of 13%.

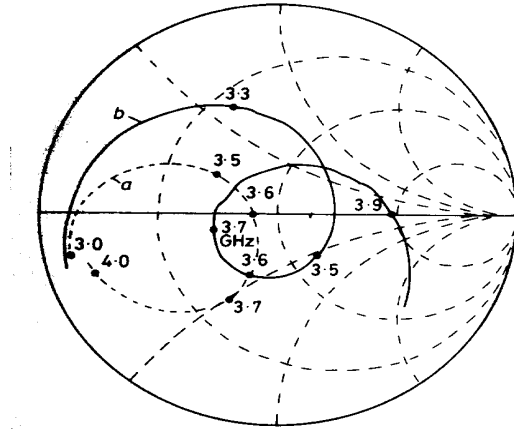


**Figure 5.12.** Smith chart of measured input impedance locus for the MSA specified in Table 5.7 when (a) no tuning stub is present (dashed curve) and (b) when the tuning stub specified in Table 5.7 is present (solid curve) [11]

The E-plane radiation pattern of the proximity coupled MSA is the same as that of a standard MSA with a contacting feed unless a standing wave exists on the feedline. This occurs at certain frequencies within the band. The effect is increased by the presence of the tuning stub. A longer tuning stub increases the effect. The H-plane pattern of the antenna was well formed at all frequencies. [11] In Chapter 6, a proximity coupled MSA is designed at 915 MHz, and its performance is fully characterized.

Another type of MSA that uses a non-contacting feed is the aperture coupled MSA, shown in Figure 5.13.

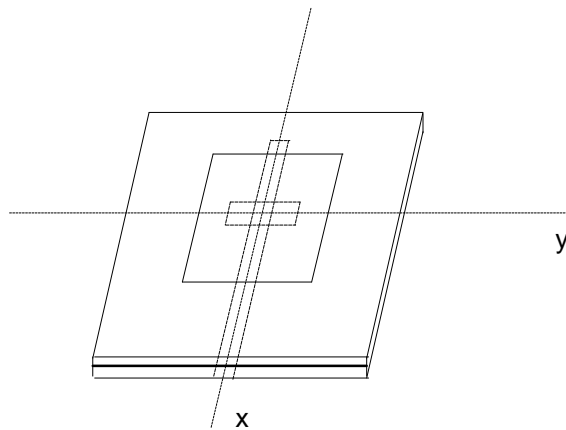


**Figure 5.13.** An aperture coupled rectangular patch MSA

The aperture coupled MSA in Figure 5.13 uses two parallel dielectric layers separated by a ground plane. The lower dielectric layer is called the substrate and the upper dielectric layer is called the superstrate. The patch is printed on top of the superstrate. The feedline is located on the bottom of the substrate. An aperture of arbitrary shape, typically a narrow rectangular slit, is cut into a ground plane located between the dielectric layers. The feedline is coupled through the aperture. [10]

This configuration allows the feedline and the antenna to use different substrates. Optimally, a microstrip feedline is printed on a thin substrate with a high dielectric constant to limit spurious feedline radiation. On the other hand, antennas operate best on thick substrates with low dielectric constant. Such a substrate maximizes radiation and thus antenna radiation efficiency. [10] The aperture coupled antenna allows the feedline and antenna to use different substrates. Thus, the performance of both is optimized. In addition, the ground plane between the antenna and feedline isolates the patch radiator from feed radiation and surface waves. This leads to better polarization purity and radiation patterns. [10]

A simplified analysis of the aperture coupled MSA in Figure 5.13 involves the magnetic cavity model, as described in Section 5.2.1. Following the work in [12], the patch and its periphery are modeled as a resonant magnetic cavity. The fields are written for the dominant  $TM_{10}$  mode. The polarization currents in a small circular aperture are written using the small-hole coupling theory in [13]. The coupling to the aperture is maximum along the x-axis at the edges of the patch and minimum at the patch center. [12] In addition, as the aperture is moved from the edge of the patch to the center, the coupling mechanism changes from a pure electric dipole to a combination of a magnetic and electric dipole, to a pure magnetic dipole. [12] Once the polarization currents in the aperture are known, the fields under an infinitely long microstrip line are solved, and the coupling coefficients between the line and the cavity fields are derived.

Calculations have shown that the coupling due to the magnetic dipole is three times greater than the electric dipole coupling. Thus, the aperture should be located along the x-axis at the center of the patch to optimize coupling. In addition, the coupling from long, thin elliptical apertures is ten times greater than that from the small circular aperture.

This indicates that a long thin rectangular aperture parallel to the width of the patch is the ideal aperture shape. [12]

An aperture coupled MSA like that illustrated in Figure 5.13 was built using the specifications in Table 5.8. The feedline impedance of the antenna specified in Table 5.8 was  $50 \Omega$ . The line extended 12 mm past the aperture and was terminated as an open circuit. [12] In this example, the dielectric constants and thicknesses of both substrates are identical to simplify analysis. Optimal performance is achieved for a thick antenna substrate with low  $\epsilon_r$  and a thin feedline substrate with high  $\epsilon_r$ . The impedance of the antenna specified in Table 5.8 was measured, and is illustrated in Figure 5.14. The portion of the feedline that extends past the aperture acts like an open-circuit stub. The impedance in Figure 5.14 was tuned for maximum bandwidth by adjusting the length of the stub. [12] Adjusting the size of the aperture also tunes the impedance of the antenna. However, the size of the aperture should be minimized in order to shield the patch radiator from feed effects. [12] The far-field radiation patterns of the aperture coupled MSA are identical to those of a standard MSA with a contacting feed. [12]

**Table 5.8.** Specifications of an aperture coupled rectangular MSA

Quantity	Value	Unit
Resonant Frequency	2.14	GHz
Patch Length	40	mm
Patch Width	30	mm
Aperture Radius	4.7	mm
Feedline substrate thickness	1.6	mm
Feedline substrate $\epsilon_r$	2.55	--
Antenna substrate thickness	1.6	mm
Antenna substrate $\epsilon_r$	2.55	--
Line Width	4.7	mm

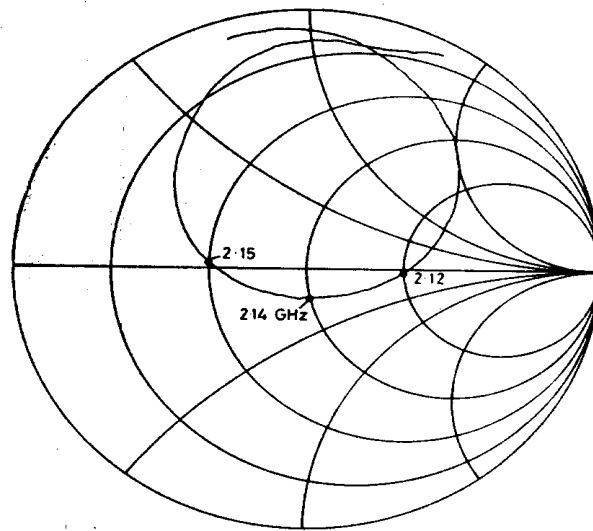


**Figure 5.14.** The input impedance of an aperture fed rectangular patch MSA.

This section outlined three methods used to enhance the bandwidth of the MSA. Other techniques exist and are found in the literature. [5,10] The following section

describes methods used to reduce the length and width of the MSA by altering the classic patch shapes.

## **5.4 Size-Reduced Microstrip Antennas**

### **5.4.1 Size-Reduced Rectangular Patch Microstrip Antennas**

The resonant rectangular patch antenna is on the order of  $\lambda/2$  in extent. The length of the element is reduced by a factor of two if the half-wave patch is short-circuited to ground at the zero potential plane. The result is a resonant rectangular patch with length on the order of  $\lambda/4$ , called a quarter-wave patch. Certain applications require further size reduction. In these cases, the shape of the patch is altered to achieve acceptable performance from rectangular patches with resonant length less than  $\lambda/4$ .

One method used to reduce the resonant length of the rectangular patch is to partially short the zero potential plane. This, as shown in Figure 5.15, increases the effective path length of the currents on the surface of the patch, and thus decreases the resonant frequency of the antenna. In Figure 5.15, the shorting stub and feed are centered on the x-axis. The ground plane dimensions are nearly the same as those of the patch. The input impedance and resonant frequency of the partially short-circuited MSA in Figure 5.15 are controlled by changing the width of the shorting stub. As the stub decreases in size, the inductance of the patch increases. This corresponds to a reduction of resonant frequency. [14] An antenna like that in Figure 5.15 was built and measured. The specifications of the antenna are given in Table 5.9.

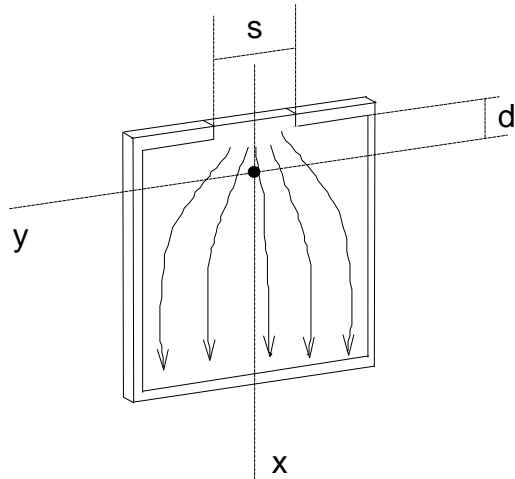


**Figure 5.15.** Currents on a rectangular patch MSA with a partial short circuit

**Table 5.9.** Specifications of a partially shorted rectangular patch MSA. [14]

Quantity	Value	Unit
Resonant Frequency	1.262	GHz
Patch Length	40	mm
Patch Width	40	mm
Substrate Material	Duroid	--
Dielectric Constant	2.20	--
Substrate Thickness	1.27	mm
Feed Point Location, $d$	varies	--
Shorting Stub Width, $s$	varies	--

The antenna specified in Table 5.9 was measured with different values of shorting stub width,  $s$ , and feed point location,  $d$ . [14] In each case, the location of the feed was adjusted to provide an impedance match to a  $50 \Omega$  coaxial line. The results are summarized in Table 5.10.

**Table 5.10.** Antenna characteristics for different shorting stub widths [14]

Case	$s$ (% of patch width)	$d$	Resonant Frequency, $f_r$ (% reduction of $f_r$ )
1	4 cm (100 %)	0.65 cm	1262 MHz (100 %)
2	3 cm (75 %)	0.60 cm	1200 MHz (95 %)
3	2 cm (50 %)	0.40 cm	1108 MHz (87.8 %)
4	1 cm (25 %)	0.35 cm	967 MHz (76.6 %)
5	0.3 cm (7.5 %)	0.10 cm	823 MHz (65 %)

Table 5.10 shows that size reductions of up to 65% (case 5) of the fully shorted rectangular patch length are possible using a partially shorted edge. [14] Further reductions in short-circuit stub width make a  $50 \Omega$  match impossible because the required feed point is too close to the shorting stub. The measured impedance of the partially shorted rectangular patch MSA between 800 and 880 MHz with a 0.3 cm shorting stub (case 5) is illustrated in Figure 5.16.

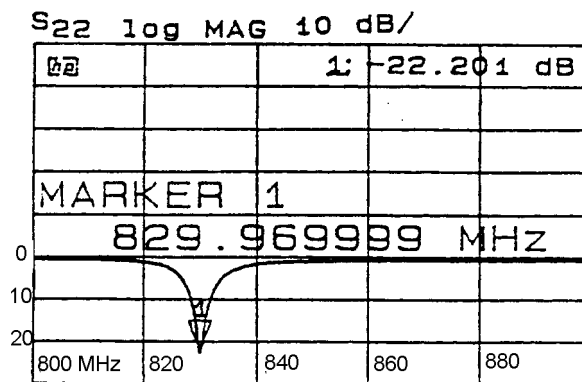


**Figure 5.16.** The measured input impedance of a partially shorted rectangular patch MSA. [14]

As shown in Figure 5.16, the bandwidth of the partially shorted antenna is less than 1% of the resonant frequency, and is narrower than that of the rectangular patch MSA with a fully shorted edge. However, the resonant length of the partially shorted antenna is one-third that of the quarter-wave patch. [14]

A variation on the partially short circuited rectangular patch MSA is the partially shorted double-C MSA. Variations on the double-C MSA are illustrated in Figure 5.17. [15] The extent of the conventional double-C MSA, shown in Figure 5.17(a), is reduced by a factor of two by short circuiting the antenna to ground at the zero potential plane. The short circuited double-C MSA is shown in Figure 5.17(b). Further size reduction is possible if the short circuited section is replaced by a partial short. [15] The antenna is fed using a coaxial probe and the feed is centered with respect to patch width. The position of the feed point is varied to tune the antenna to a 50  $\Omega$  line.

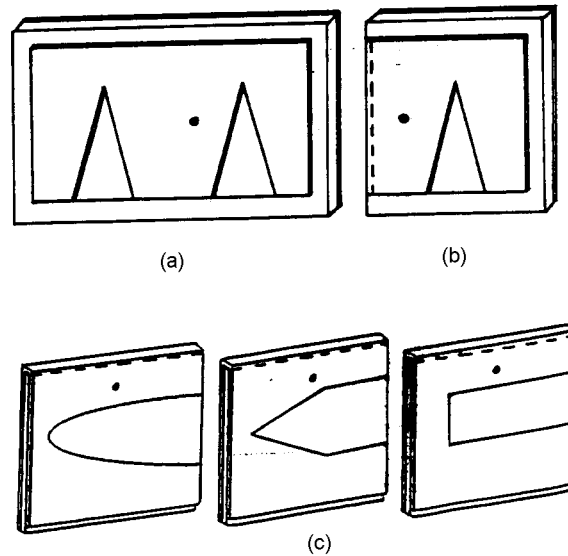


**Figure 5.17.** (a) A conventional double-C MSA. (b) A short-circuited double-C MSA  
(c) Short-circuited double-C MSA designs with different aperture shapes. [15]

Although a number of aperture shapes are possible, as shown in Figure 5.17(c), the greatest size reduction is obtained using the rectangular aperture. [15] A double-C MSA with a rectangular aperture is illustrated in Figure 5.18.

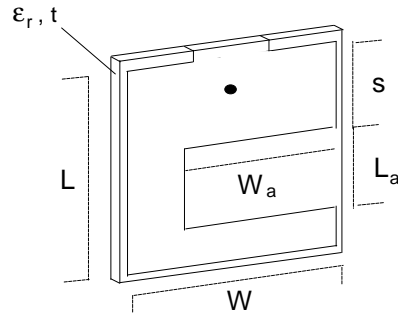


**Figure 5.18.** A shorted double-C MSA with a rectangular aperture shape. [15]

The antenna in Figure 5.18 has an aperture width,  $W_a$ , and an aperture length,  $L_a$ . The dimensions of the ground plane are very nearly those of the patch. Both aperture dimensions affect the input impedance and resonant frequency of the antenna. [15] Specifically, a reduction in aperture length increases antenna inductance and decreases resonant frequency. Reducing the length of the aperture by more than 20% of the overall length of the patch causes a degradation of radiation efficiency. Increasing the width of the aperture increases the input inductance, and considerably reduces the resonant frequency of the antenna. The radiation efficiency is degraded if the width of the aperture is greater than 75% of the width of the antenna. In addition, moving the location of the aperture closer to the shorted edge slightly reduces the resonant frequency of the antenna. [15]

A double-C MSA with the geometry illustrated in Figure 5.18 was built with the specifications listed in Table 5.11. [15]

**Table 5.11.** Specifications of a short circuited double-C MSA [15]

Quantity	Symbol	Value	Unit
Resonant Frequency	$f_r$	1.024	GHz
Patch Length	$L$	37.5	mm
Patch Width	$W$	37.5	mm
Substrate Material		Duroid 5880	--
Dielectric Constant	$\epsilon_r$	2.20	--
Substrate Thickness	$t$	1.27	mm
Aperture Location	$s$	9	mm
Aperture Length	$L_a$	10	mm
Aperture Width	$W_a$	26	mm

The antenna specified in Table 5.11 was built and measured. The input impedance of the antenna is shown in Figure 5.19 in terms of return loss.

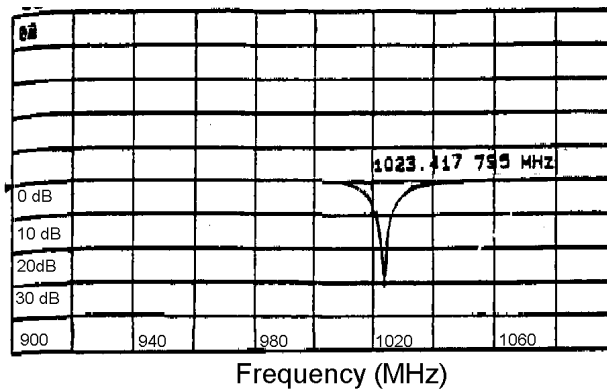


**Figure 5.19.** Return loss measurement for the double-C MSA specified in Table 5.11. [16]

Figure 5.19 shows that the double-C MSA has a narrow impedance bandwidth (return loss > 10 dB) that is about 1 % of the center frequency. For an application such as cellular PCS, a much wider bandwidth is required.

A solution to the bandwidth problem of the double-C antenna is to add in-plane parasitic patches to the double-C MSA configuration. [16] Such a design is illustrated in Figure 5.20. The conceived position of the antenna in a hand-set is also illustrated.

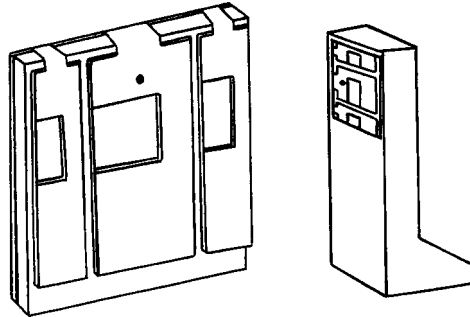


**Figure 5.20.** A double-C MSA with in-plane parasites and its application to a mobile hand-set.

[16]

The center element of the antenna in Figure 5.20 is fed using a coaxial probe that is centered with respect to the patch width,  $W$ . The other two elements are gap-coupled parasitically. The Double-C MSA with in-plane parasitic elements is illustrated in Figure 5.21.

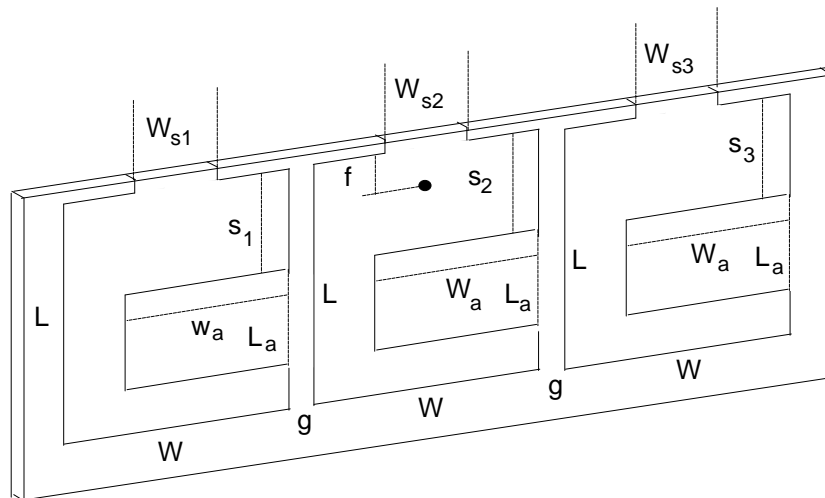


**Figure 5.21.** Dimensions of the double-C patch antenna with in plane parasitic elements [16]

The three elements are the same size, and have identical rectangular apertures. The short circuit width, and the distance between the short circuit and the apertures are adjusted on

each element to tune the input impedance. [16] The antenna in Figure 5.20 was designed using the specifications in Table 5.12. The antenna specified in Table 5.12 was optimized for impedance bandwidth. The parasitic elements were designed to resonate at frequencies closely spaced with the resonant frequency of the driven element. The coupling between the elements is increased by the edge effects in the apertures. The increased coupling makes it possible to reduce the widths of the parasitic elements. [16] However, the addition of two parasitic elements to the double-C configuration in Figure 5.18 obviously increases the width of the antenna. This disadvantage of the double-C with in plane parasitic elements stresses the trade-off between impedance bandwidth and antenna size. The antenna described by Table 5.12 was built and the measured impedance is illustrated in Figure 5.22. The impedance locus on the Smith chart in Figure 5.22 indicates a triple resonance tuned to the center of the chart. This is a wide-band frequency characteristic. The return loss plot also shows a triple resonance. The impedance bandwidth below 10 dB return loss is between 870 and 920 MHz. This corresponds to a impedance bandwidth of about 5.5 %.

**Table 5.12.** Specifications of a double-C MSA with in-plane parasitic elements

<b>Quantity</b>	<b>Value</b>	<b>Unit</b>
Resonant Frequency	900	MHz
L	42	mm
W	14	mm
g	1.5	mm
L <sub>a</sub>	11	mm
W <sub>a</sub>	9	mm
S <sub>1</sub>	11	mm
S <sub>2</sub>	10	mm
S <sub>3</sub>	9	mm
W <sub>s1</sub>	4	mm
W <sub>s2</sub>	6	mm
W <sub>s3</sub>	8	mm
f	4	mm
Substrate Material	Duroid 5880	--
Dielectric Constant	2.20	--
Substrate Thickness	2.3	mm

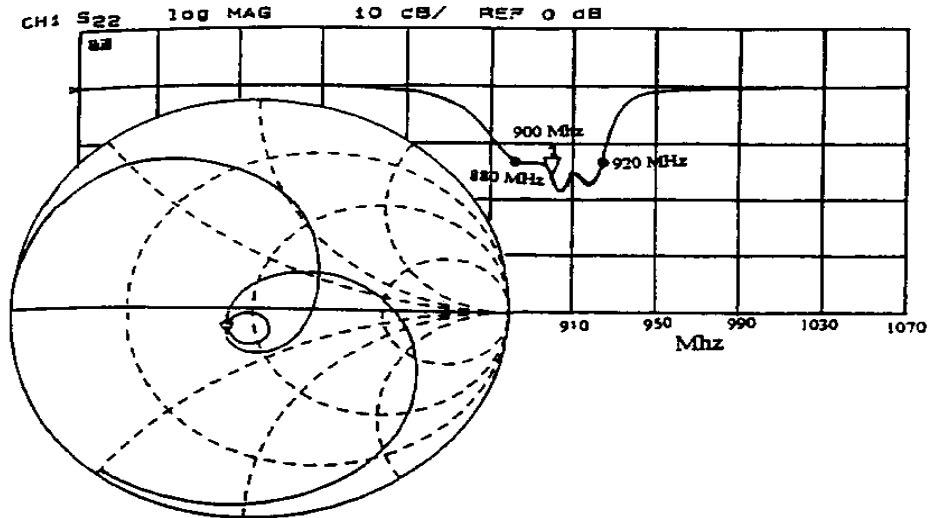


**Figure 5.22.** Smith chart and return loss representation of the input impedance of the antenna specified in Table 5.12.

In practice, it is not easy to manufacture a solid shorting plate. Therefore, the shorting plate is often replaced by a number of shorting posts. [14] This has an effect on the input impedance of the partially shorted MSA. Specifically, a series inductance and a shunt capacitance is added. The inductance is due to the self inductance of the posts. The capacitance is due to the close proximity of the posts. The addition of capacitance to the input impedance of the patch increases the resonant frequency. Therefore, it is desirable to space the posts as far apart as possible. Experiments show that the partially shorted rectangular patch MSA requires three shorting posts to simulate the continuous short circuit. [14] The feedpoint required for a  $50 \Omega$  match is changed significantly when the continuous short is replaced by the shorting posts. Table 5.13 illustrates the results of the same experiment summarized in Table 5.10 when the continuous short circuit is replaced with either three or five shorting posts.

**Table 5.13.** Antenna characteristics for partially shorted rectangular patch MSAs using shorting posts instead of a continuous short circuit. [14]

<b>Short Circuit Width</b>	<b>Resonant Frequency</b>		
	<i>Continuous Short Circuit</i>	<i>3 Shorting Pins</i>	<i>5 Shorting Pins</i>
4 cm (100 %)	1262 MHz (100 %)	1064 MHz (84.3 %)	1137 MHz (90.1 %)
3 cm (75 %)	1200 MHz (95 %)	1106 MHz (87.6 %)	1178 MHz (93.3 %)
2 cm (50 %)	1108 MHz (87.8 %)	1095 MHz (86.8 %)	1132 MHz (89.7 %)
1 cm (25 %)	967 MHz (76.6 %)	988 MHz (78.3 %)	1006 MHz (79.7 %)
0.3 cm (7.5 %)	823 MHz (65 %)	not possible	not possible

The inductive and capacitive effects of the shorting posts are evident in Table 5.13. For wider post placement, the self inductance of the posts causes a reduction of resonant frequency. As the posts come closer together, the added capacitance begins to cancel the size reduction effects. [14] The smallest stub size was not possible because the spacing between the stubs became too small.

The discussion to this point has focused on methods used to size reduce the rectangular patch antenna. It is also possible to alter the shape of the circular patch MSA to achieve size reduction and bandwidth enhancement. The subject of the next section is size-reduction of the MSA.

### 5.4.2 Size-Reduced Circular Patch Microstrip Antennas

In Figure 5.23, two sectoral sections of a circular patch are removed, and shunted with conducting strips.

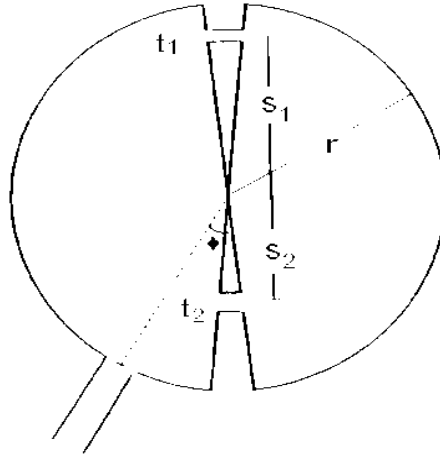


**Figure 5.23.** The dimensions of a two section sectoral circular patch MSA

In Figure 5.23,  $t$  is the slot thickness, and  $s$  is the distance of the shunting strip from the center of the patch;  $r$  is the radius of the patch and  $\phi$  is the angle between the center of the sectoral section and the feed. The sectoral slot angle is the angle between the center line and edge of the sectoral section.

The effect of removing the sectoral sections from the circular patch is to alter the current distribution on the surface of the patch. [17] Normally, the current distribution on the surface of a circular patch MSA is constant in the spherical dimension  $\phi$ . Since the current at the edge of the patch is low, the input impedance seen by a microstrip edge feed is high. [17] The result of removing the sectoral sections, and adding the shunting stubs, is a wide variation of current along the edge of the patch. Thus, it is possible to tune the input impedance of a microstrip edge-feed to  $50 \Omega$  by changing the position of the shunt stubs and feed point. [17] In addition, the circumference of the patch is lengthened by the removal of the sectoral sections. [17] This allows the sectoral circular patch antenna to have a lower resonant frequency and subsequent size reduction. In practice, the two section sectoral circular patch antenna is 19% smaller than a classic circular patch antenna

with the same resonant frequency. [17] The sectoral circular MSA illustrated in Figure 5.23 was built with the specifications listed in Table 5.14.

**Table 5.14.** Specifications of a short circuited double-C MSA

Quantity	Value	Unit
Resonant Frequency	677.5	MHz
r	49.5	mm
s <sub>1</sub>	40	mm
s <sub>2</sub>	20	mm
t <sub>1</sub>	4	mm
t <sub>2</sub>	6	mm
φ	20	°
Slot Angle	6	°
Substrate Dielectric constant	4.5	
Substrate Thickness	1.6	mm

The input impedance of the circular sectoral MSA specified in Table 5.14 is shown in terms of VSWR in Figure 5.24. Figure 5.25 shows the co-polarized and cross-polarized far-field radiation patterns of the antenna in the E and H-planes.

Figure 5.24 shows that the antenna is very well matched at 677.5 MHz. The VSWR at resonance is 1.04. The impedance bandwidth of the antenna below a VSWR of 2 is 13 MHz or 2.3 % of the resonant frequency. The 3 dB beamwidth of the E-plane pattern is 94°. The 3 dB beamwidth of the H-plane pattern is 70°. The cross polarization level at boresight is at least -10 dB. [17] The high cross-polarization level indicates that the antenna is polarization insensitive. This feature is attractive in the hand-held environment.

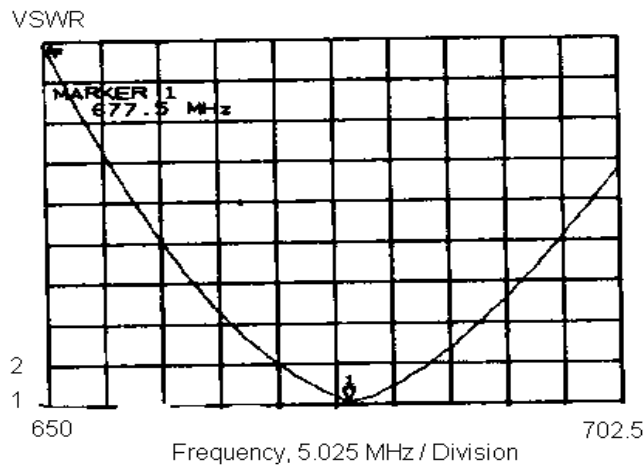


**Figure 5.24.** Measured VSWR of the sectoral circular MSA antenna specified in Table 5.14. [17]

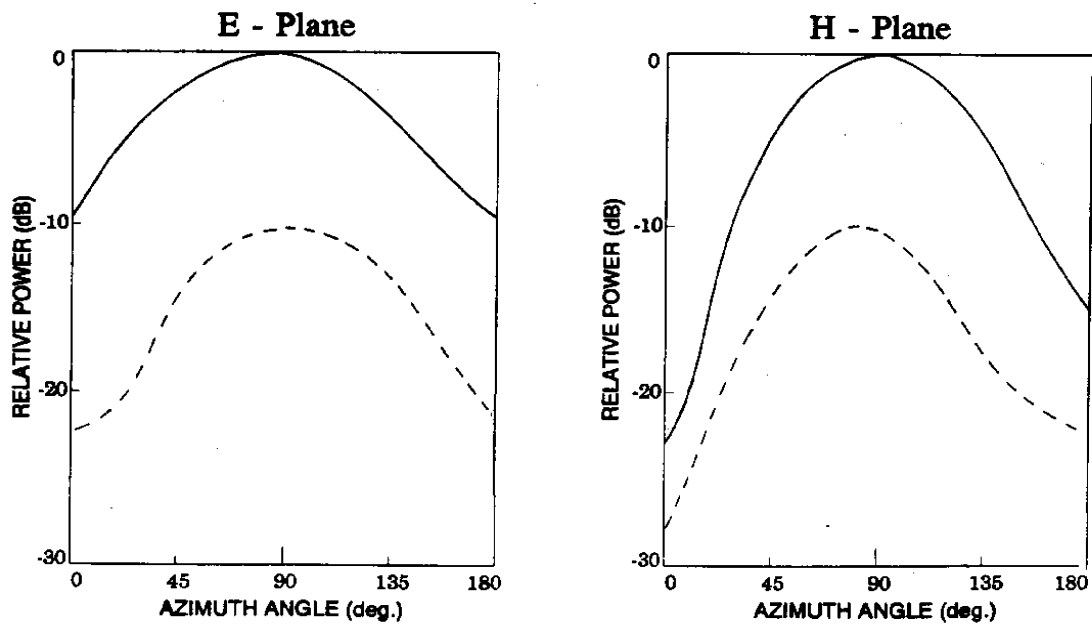


**Figure 5.25.** Far-field radiation patterns of the sectoral circular microstrip antenna specified in Table 5.14. Solid Curve is the co-polarized pattern. Dashed Curve is the cross-polarized pattern. [17]

It is possible to increase both the beamwidths and impedance bandwidth of the antenna in Figure 5.23 by removing two more sectoral sections. [18] The resulting antenna is illustrated in Figure 5.26.

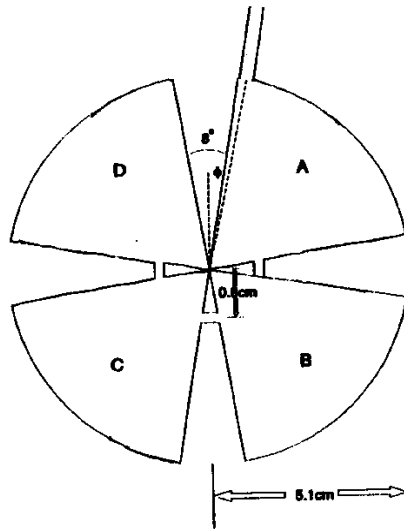


**Figure 5.26.** Dimensions of a four quadrant circular sectoral patch antenna [18]

The antenna in Figure 5.26 was built using the dimensions noted in the figure and measured. Figure 5.27 shows the VSWR at the feed point of the antenna.

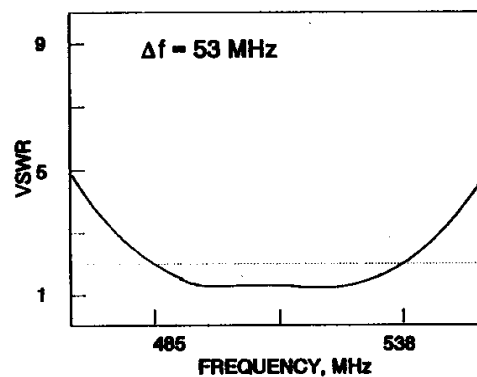


**Figure 5.27.** VSWR of the sectoral circular patch antenna specified in Figure 5.26 calculated using the FDTD technique. [18]

Figure 5.27 shows that the four section circular sectoral patch antenna is well matched over a wide impedance bandwidth. The impedance bandwidth below a VSWR of 2 is 10.35% of the center frequency. Thus this size-reduced antenna design has broadband characteristics. The resonant frequency of the antenna is 511.59 MHz. This corresponds to a size reduction factor of 59.8 % with respect to a conventional circular patch antenna of

the same dimension. Figure 5.28 shows the far-field radiation patterns in the E and H-planes.

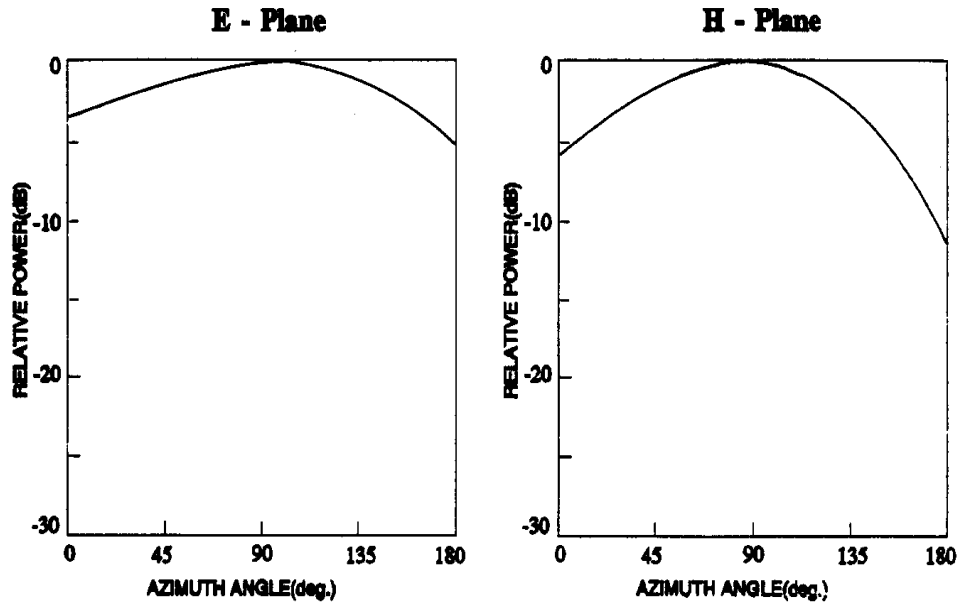


**Figure 5.28.** Far-field radiation patterns of the sectoral circular patch antenna specified in Figure 5.25 measured using the FDTD technique. [18]

The 3 dB beamwidth of the E-plane pattern in Figure 5.28 is  $126^\circ$  and that of the H-plane pattern is  $75^\circ$ . [18]

In comparison, the four quadrant circular sectoral antenna in Figure 5.26 shows increased size reduction, better impedance bandwidth, and wider beamwidths in both planes compared with the two quadrant design in Figure 5.23.

## 5.5. Summary of Broad Band and Size-Reduced Microstrip Antenna Designs

Sections 5.3 and 5.4 discussed methods used to increase the impedance bandwidth and decrease the dimensions of the microstrip antenna. In Table 5.15, the antenna designs in Sections 5.3 and 5.4 are summarized for reference.

**Table 5.15.** Summary of Wide Band and Size-Reduced Antenna Designs

#	Antenna Name	Figure Illustrating Geometry	Dimensions	$f_{\text{resonant}}$ (GHz)	VSWR or Return Loss at Resonance	BW (% $f_{\text{resonant}}$ )
<i>Wide Band Microstrip Antenna Designs</i>						
1	Stacked Patch (circular)	5.8	Diameter = 68 mm $t_{\text{substrate}} = 1.524$ mm air gap = 20.5 mm	1.62	39 dB (return loss)	5.6 %
2	Stacked Patch (rectangular)	5.10	Length = 10 mm Width = 15 mm $t_{\text{substrate}} = 1.524$ mm air gap varies	10	varies Table 5.6	varies Tb. 5.6
3	Proximity Coupled MSA	5.11	Length = 25 mm Width = 40 mm	3.5	---	13 %
4	Aperture Coupled MSA	5.13	Length = 40 mm Width = 30 mm	2.14	---	$\approx 1\%$
<i>Size-Reduced Microstrip Antenna Designs</i>						
5	Partially Shorted MSA (rectangular)	5.15	Length = 40 mm Width = 40 mm	1.26 - 0.823	22 dB (return loss)	< 1%
6	Double-C Patch	5.18	Length = 37.5 mm Width = 37.5 mm	1.024	30 dB (return loss)	1 %
7	Double-C with Parasitics	5.21	Length = 42 mm Total Width=42 mm	0.900	18 dB (return loss)	5.5 %
8	Two Section Circular Sectoral Patch	5.23	Radius = 49.5 mm	0.678	1.04 (VSWR)	2 %
9	Four Section Circular Sectoral Patch	5.26	Radius = 51 mm	0.512	---	10.35%

## 5.6. Conclusion

This chapter discussed the design of canonical, broadband, and size-reduced microstrip antennas (MSAs). The magnetic cavity model was presented as a design tool and was applied to the circular and rectangular patch MSA designs. Design formulas were derived using the magnetic cavity model for the circular and rectangular patch antennas. Techniques to increase the impedance bandwidth of the MSA were described. Finally, size reduction methods for rectangular and circular patch antennas were treated.

Since the 1970s, the demand for low-profile, light, inexpensive, conformal antennas has driven extensive research into the MSA. Complete discussions are found in a number of sources. [19, 20, 21] In the next chapter a numerical technique is developed that is applicable to planar microstrip antennas. The algorithm is applied using a commercially available software package called SONNET to perform a numerical study of the proximity coupled rectangular patch antenna.

## REFERENCES FOR CHAPTER 5

### Early Microstrip Literature (Not Referenced)

Deschamps, G. A. "Microstrip Microwave Antennas". presented at the Third USAF Symposium on Antennas, 1953.

Gutton, H., Baissinot, G. "Flat Aerial for Ultra-high Frequencies" French Patent no. 703 113, 1955

Munson, R.E. "Single Slot Cavity Antennas Assembly". U.S. Patent no. 3713162, Jan. 23, 1973.

Munson, R. E. "Conformal Microstrip Antennas and Microstrip Phased Arrays". *IEEE Transactions on Antennas and Propagation*, v. AP-22, 1974, pp. 74-78.

Howell, J. Q. "Microstrip Antennas". *Digest of the International Symposium of the Antennas and Propagation Society*, Williamsburg, VA, Dec. 1972, pp. 172-180.

Howell, J.Q. "Microstrip Antennas". *IEEE Transactions on Antennas and Propagation*, v. AP-23, Jan. 1975, pp. 90-93.

## Referenced Sources:

1. Carver, K. R., Mink, J. W. "Microstrip Antenna Technology". *IEEE Transactions on Antennas and Propagation*, v. AP-29, Jan. 1981, pp. 2-24.
2. Jellett, S. T., Bialkowski, M. E., Dimitrios, A. P. "An Experimental Investigation into Microstrip Antenna Elements Suitable for Mobilsat Applications". *Microwave and Optical Technology Letters*, v. 6, n. 4, March 1993.
3. Hirasawa, K., Haneishi, M. (eds.), *Analysis, Design, and Measurement of Small and Low-Profile Antennas*. Chapter 4: Suzuki, Y. "Key Points in the Design and Measurement of Microstrip Antennas". Artech House, Boston, 1992.
4. Hirasawa, K., Haneishi, M. (eds.), *Analysis, Design, and Measurement of Small and Low-Profile Antennas*. Chapter 3: Haneishi, M. "Evaluation of the Basic Performance of Microstrip Antennas". Artech House, Boston, 1992.
5. Sanchez-Hernandez, D., Robertson, I. D., "A Survey of Broadband Microstrip Patch Antennas". *Microwave Journal*, Sept. 1996, pp. 60-82.
6. Sanad, M. "Microstrip Antennas on Very Small Ground Planes for Portable Communication Systems". *Proceedings of the IEEE Antennas and Propagation Society Symposium*, June 1994, pp. 810-813.
7. Vandenbosch, G. A. E., Van de Capelle, A. "Study of the Capacitively Fed Microstrip Antenna" *IEEE Transactions on Antennas and Propagation*, v. 42, n. 12, Dec. 1994.
8. Long S. A., Walton, M. D., "A Dual-Frequency Stacked Microstrip Antenna". *IEEE Transactions on Antennas and Propagation*, v. AP-27, n. 2, 1979, pp. 270-273.
9. Lee, R. Q., Lee K. "Experimental Study of the Two-Layer Electromagnetically Coupled Rectangular Patch Antenna". *IEEE Transactions on Antennas and Propagation*, v. 38, n. 8, Aug. 1990.
10. Pozar, D. M., "Microstrip Antennas". *Proceedings of the IEEE*, v. 80, n.1, Jan. 1992.
11. Pozar, D. M., Kaufman, B. "Increasing the Bandwidth of a Microstrip Antenna by Proximity Coupling". *Electronics Letters*, v. 23, Apr. 1987, pp. 368-369
12. Pozar, D. M., "Microstrip Antenna Aperture Coupled to a Microstrip Line". *Electronics Letters*, v. 21, n. 2, Jan. 1985, pp. 49-50.
14. Sanad, M. "A Small Size Microstrip Antenna Having a Partial Short Circuit". *IEEE International Conference on Antennas and Propagation*, v. 1, April 1995, pp. 282-286.
15. Sanad, M. "Double C-Patch Antennas Having Different Aperture Shapes". *IEEE Antennas and Propagation Symposium Digest*, June 1995, pp. 2116-2119.
16. Sanad, M. "A Wide Band Microstrip Antenna for Portable Cordless Telephones". *IEEE Antennas and Propagation Symposium Digest*, June 1995, pp. 1132-1135.

17. Dey, D., Aanandan, C. K., Mohanan, P, Nair, K. G. "A New Compact Circular Patch Antenna". *Proceedings of the IEEE Antennas and Propagation Society Symposium*, June 1994, pp. 822-825.
18. George, J., Mohanan, P, Nair, K. G. "A Broad Band Low Profile Microstrip Circular Patch Antenna". *Proceedings of the IEEE Antennas and Propagation Society Symposium*, June 1995, pp. 700-703.
19. Bahl, I. J., Bhartia, P. *Microstrip Antennas*. Artech House, Norwood MA, 1980.
20. James, J. R. et al. *Microstrip Antenna Theory and Design*, Peter Peregrinus Ltd, London, 1981.
21. James, J.R., Hall, P. S. (eds.) *Handbook of Microstrip Antennas*. Peter Peregrinus Ltd. (London) on behalf of the IEE, v. 1 & 2, 1989.